X-ray diffraction study of thermal stress relaxation in ZnO films deposited by magnetron sputtering

Florine Conchon, Pierre-Olivier Renault, Éric Le Bourhis, Christopher Krauss, Philippe Goudeau, Etienne Barthel, Sergey Y. Grachev, Elin Sondergard, Véronique Rondeau, René Gy, et al.

Manuscript Cover page

Paper Reference Number: #133 (program number CP-3)

Title of Paper: X-ray diffraction study of thermal stress relaxation in ZnO films deposited by magnetron sputtering

Corresponding Author: Pierre-Olivier RENAULT

Full Mailing Address:

Institut P', Espace Phymat, CNRS-Universite de Poitiers UPR 3346, SP2MI, BP 30179, 86962 Futuroscope France

Telephone: 33 5 49 49 67 45

Fax: 33 5 49 49 66 92

Email: pierre.olivier.renault@univ-poitiers.fr

Keywords : Zinc oxide, magnetron sputtering, X-ray diffraction, residual stresses, thermal relaxation.

Estimation of the length of the manuscript

			Number of words
Length of the text			4561
Number of Tables	0	x 150	
Number of Figures	5	x 150	750
Total number of words			5311

Author's certification

International Conference on Metallurgical Coatings and Thin Films

April 26-30, 2010

This is to certify that I have obtained the necessary authorization for publication of the enclosed paper # 133 in the ICMCTF 2010 Conference and in Thin Solid Films and that the paper is original and unpublished and is not being considered for publication elsewhere.

Corresponding Author

Pierre-Olivier Renault
University of Poitiers

X-ray diffraction study of thermal stress relaxation in ZnO films deposited by magnetron sputtering

F. Conchon[a], P.O. Renault[a*], E. Le Bourhis[a], C. Krauss[a], P. Goudeau[a],
E. Barthel[b], S. Yu. Grachev[b], E. Sondergard[b],
V. Rondeau[c], R. Gy[c], R. Lazzari[d], J. Jupille[d], N. Brun[e]

a Institut P', Université de Poitiers -Ensma-UPR CNRS 3346, 86962 Futuroscope, France
b Lab. Surface du Verre et Interfaces (SVI), UMR 125, 93303 Aubervilliers, France
c Lab. Recherche de Saint-Gobain (SGR), 93303 Aubervilliers, France
d Institut des Nanosciences de Paris (INSP), UMR 7588, 75015 Paris, France
e Lab. Physique des Solides (LPS), UMR 8502, 91405 Orsay, France

Abstract

X-ray diffraction stresses analyses have been performed on two different thin films deposited onto silicon substrate: ZnO and ZnO encapsulated into Si_3N_4 layers. We showed that both as-deposited ZnO films are in a high compressive stress state. In situ x-ray diffraction measurements inside a furnace revealed a relaxation of the as-grown stresses at temperatures which vary with the atmosphere in the furnace and change with Si_3N_4 encapsulation. The observations show that Si_3N_4 films lying on both sides of the ZnO film play an important role in the mechanisms responsible for the stress relaxation during heat treatment. The different temperatures observed for relaxation in ambient and argon atmospheres suggest that the thermally activated stress relaxation may be attributed to a variation of the stoichiometry of the ZnO films. The present observations pave the way to fine tuning of the residual stresses through thermal treatment parameters.

* Author to whom any correspondence should be addressed: pierre.olivier.renault@univ-poitiers.fr

1. Introduction

ZnO has been studied increasingly for several years in regard to its particular and original properties. The extreme complexity of intrinsic defects seemed to limit the studies in the past, but now these properties become advantageous in the scope of material science [1]. Many studies deal with electronic and optical properties [2-6], and to much less extend with stresses building in ZnO thin films [6-8]. Nowadays, ZnO, being optically transparent, is widely used in many application domains such as ultraviolet detectors, light-emitting diodes, solar cells. As a II-VI semiconductor, ZnO physical properties (direct gap around 3.3 eV at room temperature [9]) found applications in short-wavelength optoelectronic devices and surface protection. The growth of ZnO films can be realized with several deposition techniques such as, non exhaustively, sputtering methods [10], metal-organic chemical vapor deposition [11] and pulsed laser deposition [12]. Each cited layering method induces residual stresses which can be detrimental for the film quality and cause spontaneous delamination at either short or long term. These stresses can also have large effects on the electrical and optical properties of the ZnO films [13-16]. It is thus of utmost importance to get insight into the stresses building in the films during the deposition process. The generation of stresses is strongly linked to the deposition process, to the microstructure of the thin film and the nature of the interfaces.

The importance of all these factors varies with the experimental deposition method conditions and post-deposition treatments. In the case of magnetron sputtering, oxygen partial pressure [17] as well as r.f. power [18] affect stresses in ZnO films. Post-heat treatment is known to affect texture, grain size and surface roughness [19]. The magnetron sputtering deposition technique is often used for its large and fast surface recovering although inducing high compressive intrinsic stresses in ZnO thin films around 1GPa [6,20], which causes film degradations. This deposition technique often leads to the wurtzite structure of ZnO (P63mc) with a columnar growth associated to a (0002) preferential orientation [10]. Moreover, the grain boundaries play an

important role in electrical properties [17] and stress relaxation [21].

For all these above reasons, many studies are in progress for comprehension of stresses and relaxation mechanisms in ZnO deposits. In the present paper, X-ray diffraction measurements have been performed on two different thin films (100 nm thick) deposited onto silicon substrates: ZnO and ZnO encapsulated into Si_3N_4 layers. In-situ x-ray diffraction measurements have been performed during annealing up to 800°C with ambient and argon atmospheres inside the furnace chamber, and, ex situ x-ray stress analysis has been performed to study accurately residual stresses relaxation.

2. Experiments

Two different x-ray diffraction experiments have been performed on both samples (raw ZnO and encapsulated ZnO): in situ θ-2θ scans in a furnace on a Bruker diffractometer, ex-situ x-ray stress analysis at room temperature on a Seifert diffractometer.

2.1. ZnO films elaboration

ZnO films (100 nm thick) were deposited by magnetron sputtering on glass and (100) Si substrates covered with a native oxide. In the present paper, we report only observations on films deposited on silicon substrate because the glass induced a large halo on the diffractogram and a high background which complicate the analysis of XRD data. We used a zinc target, 40 mm apart from the substrate. Films were sputter-deposited under Ar pressure of 1.5×10^{-6} bar, with a power of 1500 W. The content of oxygen in the plasma was about 48%. The deposition was conducted without intentional substrate heating. Finally, two kinds of films deposited on Si were analyzed: raw ZnO films (100 nm thick) and ZnO films (100 nm thick) encapsulated on both sides (e.g. at the film/substrate and at the film/air interfaces) by Si_3N_4 protective layers (40 nm thick). These

Si_3N_4 sublayers are used as diffusion barriers and may also help in preventing the active film from ageing or scratching.

2.2. In-situ x-ray diffraction measurements

A first set of experiments has been performed where attention is paid to in-situ XRD measurements and their interpretation in terms of stress relaxation mechanisms. For that purpose, we performed θ-2θ scans in the 2θ range of 29-39° to observe the evolution of the peak position and shape during annealing. A four-circle Bruker D8 diffractometer is used. It is equipped with a Cu X-ray source with a linear focus, Soller slits determining the divergence (1°) of the incident beam. Finally, the diffracted beam is collected by a set-up composed by two slits (0.6 mm and 0.2 mm) and a Sol'X detector. Heat treatments were carried out on raw and encapsulated ZnO films in a hemispheric furnace mounted on the diffractometer. This furnace is equipped with a graphite dome and allows performing heat treatment under controlled atmosphere up to 1100°C. In this study, films were annealed both in argon and air atmosphere up to 800°C with a heating/cooling rate of 1°C/s. It is worth noting that the θ-2θ scans last about three hours, and relaxation processes or chemical diffusion may happen during the measurement. Moreover, it is important for such experiments to keep in mind the thermal expansion mismatch between the materials. Considering thermal expansion, ZnO is anisotropic : $\alpha_a = 8.47 \times 10^{-6}\ °C^{-1}$ (along the a axis of the hexagonal unit cell) and $\alpha_c = 4.94 \times 10^{-6}\ °C^{-1}$ (along the c axis) [22]. For the Si substrate, we have taken a mean value of $\alpha_{Si} \sim 3.45 \times 10^{-6}\ °C^{-1}$ in the present temperature range ($\alpha_a = 2.6 \times 10^{-6}\ °C^{-1}$ at room temperature and $4.3 \times 10^{-6}\ °C^{-1}$ at 800°C [22]).

2.3. Ex situ x-ray diffraction measurements

In the aim of analyzing residual stresses in thin films one can have recourse to various techniques

such as the wafer curvature technique [23,24] or Raman spectroscopy [25], but the most common non-destructive method to determine residual strains and stresses in thin films is based on XRD [26]. The 2θ shifts observed during in-situ XRD measurements can already give some idea about the level of residual stresses in the film. But quantitative reliable analysis requires data on much more than one diffraction peak shift. In the present study, residual stresses analysis was investigated by complementary XRD measurements on a four-circle Seifert 3003 diffractometer. This diffractometer is equipped with a Cu X-ray source (1×1 mm2 point focus) and a Ni filter in the direct beam path to absorb the CuKβ radiation. The incident beam is collimated with a 1 mm diameter collimator and focused on the sample mounted on a four-circle goniometer. The detector set-up is defined by two slits (0.5° and 1° of acceptance) and a proportional detector.

Residual stresses were then evaluated by the $\sin^2\psi$ method [26,27] which is described in details below. Whereas the wafer curvature technique (based on Stoney's formalism [28]) leads to the determination of the macroscopic residual stresses implying the whole film volume (crystalline and non-crystalline), the $\sin^2\psi$ method only concerns the diffracting regions of the film. The XRD stress analysis relies on the evaluation of the stress state in the material by the measurement of d-spacings in different directions of reciprocal space. This can be achieved by performing θ-2θ scans for various (14 in the present study) tilt angles ψ (ψ being the angle between the normal to the surface and the normal to the diffracting planes).

For the general case of a triaxial state of stress, the strain experienced by a set of lattice planes {hkl} in a direction defined by the azimuthal angle φ and the tilt angle ψ depends on the components of the stress tensor, σ_{ij} (i, j = 1 to 3) [27]. For sub-surface regions like thin films, the strain-stress relation can be simplified due to the free surface condition (σ_{i3} =0). This state of stress is defined as a planar (or biaxial) stress state, and using the logarithmic strain definition we

can write:

$$\varepsilon_{\varphi\psi}^{hkl} = \ln\left(\frac{d_{\varphi\psi}^{hkl}}{d_0^{hkl}}\right) = \ln\left(\frac{\sin\theta_0^{hkl}}{\sin\theta_{\varphi\psi}^{hkl}}\right) = \frac{1}{2}S_2^{hkl}\sigma_\varphi \sin^2\psi + S_1^{hkl}(\sigma_{11}+\sigma_{22}) \quad (1)$$

where S_1^{hkl} and $1/2S_2^{hkl}$ are the so-called x-ray elastic constants (XECs) [26], $d_{\varphi\psi}^{hkl}$ (corresponding to $\theta_{\varphi\psi}^{hkl}$) is the lattice plane spacing measured in the direction (φ, ψ), d_0^{hkl} the stress-free lattice spacing (corresponding to θ_0^{hkl}). Furthermore, if a rotationally symmetric stress state is present then $\sigma_{11} = \sigma_{22} = \sigma_\varphi = \sigma$ and Eq.(1) reduces to:

$$\ln\left(\frac{1}{\sin\theta_{\varphi\psi}^{hkl}}\right) = \frac{1}{2}S_2^{hkl}\sigma\sin^2\psi + 2S_1^{hkl}\sigma + \ln\left(\frac{1}{\sin\theta_0^{hkl}}\right) \quad (2)$$

For a macroscopically isotropic material, the strain (or ln(1/sinθ)) vs $\sin^2\psi$ plots are linear, the slopes being directly proportional to the stress but are hkl dependent (via the XEC see Eq. (2)). Textured materials are generally macroscopically non isotropic and this can lead to strong departures from linearity in strain vs $\sin^2\psi$ plots for some reflections [26,29]. Strong textured materials are often encountered in PVD (physical vapor deposition) films [30,31] and, when local anisotropy is combined with crystallographic texture x-ray stress analysis has to be performed with care [26,31,32]. ZnO crystallizes in a hexagonal structure (see section 3.1). Using the following values for the stiffnesses c_{ij} ($\times 10^5$ MPa): c_{11}= 2.097, c_{12}= 1.211, c_{13}= 1.052, c_{33}= 2.109, c_{55}= 0.425 [33], the elastic constants such as the Young's modulus of ZnO single crystal can be calculated: the Young's modulus in the (10-10) direction is about 127 GPa, it is about 118 GPa in the softest direction while it is 144 GPa in the stiffest direction (0001). The calculation of XECs should be related to the actual microstructure and reflects both the local anisotropy and the macroscopic anisotropy. As ZnO is locally slightly elastically anisotropic, it can be assumed as

macroscopically isotropic. Indeed, whatever the microstructure of the ZnO films, the error on the actual XECs of a polycrystalline ZnO will be of a few %. The largest error could be about 10% (depending on the considered crystallographic direction) in the case of a strong texture ZnO sample, but even in that case if the texture does not drastically change during the heat treatment the relative stress evolutions will be accepted as valid. In the present paper, the residual stresses are derived from the slope of the $\sin^2\psi$ plot expressed by Eq.(2) using XECs of $S_1^{hkl} = -2.867\times10^{-6}$ MPa and $1/2S_2^{hkl} = 10.92\times10^{-6}$ MPa.

3. Results

3.1. Microstructural considerations

The first three peaks, (10-10) (0002) and (10-11), of the hexagonal phase of ZnO (space group P63mc) are clearly identified for all the samples on the θ-2θ scans. Moreover, all ZnO films (raw and encapsulated) exhibit a preferential crystallographic orientation: a fiber texture with the main texture component (0001). This point is supported by the variation of the relative intensities on the diffractograms in Fig. 1. Indeed, the peak intensity of the (0002) reflection is higher for small ψ values than for larger ψ angles and the diffracted intensity increases around ψ=53° for the (10-11) reflection (which corresponds to the angle between the (0002) and (10-11) planes equal to 58°).

3.2. In-situ x-ray diffraction

As detailed in section 2.2, ZnO films were characterized by in-situ XRD during annealing. Each sample was analyzed both under air and under an argon flux (P = 1.3 bar) in the furnace chamber. The over pressurized experiment allows to limit the presence of oxygen although it can not be precluded. At each temperature plateau (for T= 30°C, 200°C, 400°C, 600°C, 800°C and after

cooling at 30°C) θ-2θ scans are recorded.

As shown in Fig. 2, the (0002) reflection is becoming sharper and more intense as the annealing temperature increases. This is explained by microstructural changes which appear at about 400°C. Indeed, annealing at 200°C does not induce significant changes while further heating from 400°C up to 800°C induces a large decrease of the Full Width at Half Maximum (FWHM) of the (0002) diffraction peak. This observation can be attributed to the increase of grain size and/or decrease of microstrains (defects annihilation) [26]. This FWHM evolution is similar for both raw and encapsulated ZnO films (about -50%). Concomitantly to the FWHM decrease, the enhancement of the (0002) peak intensity is observed. The integrated intensity increases by about 50% for raw ZnO while it is almost constant for encapsulated ZnO. Hence, the annealing at 800°C induces a significant change in the microstructure of ZnO thin films, the "crystallinity" is improved for both films and the (0002) fiber texture is enhanced for the raw ZnO film.

Fig. 3 shows the evolution of the (0002) peak position (which is sensitive to the out-of-plane strain) as a function of temperature for both ZnO samples and both atmospheres in the furnace chamber. Experimental data presented here have been corrected taking into account the displacement of the sample surface during heat treatment. Firstly, the starting 2θ values are smaller than that of the corresponding bulk value. Taking this latest value as the reference one, this observation means that both as-deposited ZnO films are in a compressive stress state (confirmed by ex-situ measurements). Following the same reason, all ZnO films are in a tensile stress state after the heat treatment. Indeed, the final 2θ values are larger than the one corresponding to the bulk value for the four cases. Secondly, a small decrease of 2θ is observed in the temperature range 30°C-200°C for raw ZnO (Fig. 3, full symbols) and range 30°C up to 400°C for encapsulated ZnO (Fig. 3, open symbols). This can be attributed to in-plane compressive thermal stresses arising in the ZnO film because of the difference in coefficients of

thermal expansion between the Si substrate and the ZnO film. The film having a coefficient of thermal expansion larger than that of the substrate, it is then subjected to in-plane compressive stresses upon heating giving rise to a tensile strain in the out-of-plane direction. From 200°C to 600°C, the 2θ values increase for raw ZnO. This may be attributed to a stress relaxation or/and a change in stoichiometry. In any case, the oxygen seems to be an influent parameter as the evolution is delayed for a treatment under argon atmosphere. This remark is confirmed by the fact that the presence of Si_3N_4 layers also delays stress the relaxation. Indeed, the 2θ evolutions for raw ZnO (Fig. 3, full gray triangle) and encapsulated ZnO (Fig. 3, open symbols) are similar and shifted by about 200°C. Moreover, the atmosphere inside the furnace chamber has no influence in the case of encapsulated ZnO. Lastly, 2θ values are similar for the four studied cases at 800°C and they increase by about 0.17° during cooling to room temperature. As already seen for heating, the increase of 2θ values can be attributed to high in-plane tensile thermal stresses which appear during cooling because of the difference in coefficients of thermal expansion between substrate and film.

3.3. Ex situ residual stress analysis

The $\sin^2\psi$ analysis has been carried out on both ZnO films at room temperature after each treatment used for in situ XRD except 200°C (for T= 30°C, 400°C, 600°C, 800°C and after cooling at 30°C). Typical set of diffractograms is shown in Fig. 1. In order to extract the peak position of the (10-10) (0002) and (10-11) reflections, θ-2θ scans were least-squares fitted with three Voigt functions [35] (considering a linear background). Figs. 4 show typical ln(1/sinθ) vs $\sin^2\psi$ plots. Each set of data strongly suggests linear variation as expected from Eq.(2) with the least-square fits being shown (lines in Figs. 4). These linear fits are performed by taking into account weights (represented by the errors bars) attributed to experimental points. The weights

have been calculated from the uncertainty ($\Delta 2\theta$) on the peak position which is extracted from the simulation of the θ–2θ scans.

For sake of clarity, Figs. 4 show the $\sin^2\psi$ plots only for the (10-11) reflection. As a first result, the $\sin^2\psi$ plots (Figs. 4) exhibit a linear behavior which confirms that the ZnO may be considered as macroscopically isotropic. Moreover, the negative slopes observed on the $\sin^2\psi$ plots for both as-deposited ZnO films (Figs. 4, open square) reveal that they are in a compressive stress state. Using Eq. (2), we obtain stress values of σ = -0.8 ($\pm$ 0.1) GPa for ZnO/Si and σ = -0.6 ($\pm$ 0.08) GPa for Si_3N_4/ZnO/ Si_3N_4/Si which are in good agreement with the values reported by Hinze and Ellmer on similar systems [30]. As the stress values are similar for these two kinds of samples, we can conclude that the Si_3N_4 films lying on both sides of the ZnO film have no mechanical influence on ZnO. From the mechanical point of view, this result is expected because of the small thicknesses of Si_3N_4 films. From the microstructural point of view, this result means that the Si_3N_4 underlayer has no significant influence on the growth of ZnO.

After annealing at 400°C, the compressive stress increases for the encapsulated ZnO (Fig. 4a), while the initial compressive stress state is decreasing slightly for the raw ZnO (Fig. 4b). After annealing at 600°C, there is a drastic stress relaxation for both films: encapsulated ZnO is almost stress-free (-40 MPa) while the raw ZnO stress state becomes tensile, i.e. tensile stress of about 500 MPa. Then both ZnO film tend to a similar tensile stress state of about 600 MPa after annealing at 800°C. It is worth noting that the $\sin^2\psi$ graphs for samples annealed at different temperatures (see Fig.4) do not have a common intersection point. This suggests that the stress-free lattice parameter changes (decreases!) due to annealing. It can be explained by microstructural/stoichiometry changes.

4. Discussion

Ex situ XRD measurements recorded on the annealed samples show significant changes in terms of residual stresses. Annealing strongly impacts the residual stresses which reverse from compressive to tensile for both films. These results show that Si_3N_4 films lying on both sides of the ZnO film play an important role in the kinetic responsible for the relaxation of residual stresses during heat treatment. However, the kinetic of thermal stress relaxation depends on the sample and on the atmosphere. The identification of this mechanism appears then to be a crucial point at this stage to control the value of residual stresses in these films. The explanation for the formation/relaxation of stress in oxide materials can be more complex than for metallic materials. Indeed, an important parameter comes into play when depositing thin oxide films: the stoichiometry. For sputter-deposited ZnO films, many studies concern the evolution of the stress and the microstructure as a function of the sputtering pressure and the oxygen partial pressure [10,20,36-39]. These two parameters strongly influence residual stresses in sputtered ZnO films. Moreover ZnO is well-known to present several types of point defects in large concentration. Hence, thermally-induced changes of the stoichiometry are highly probable in the ZnO films. The different behavior observed for both atmosphere (in the case of ZnO/Si) and, for both samples (with or without Si_3N_4 protective layers) suggests that the stress relaxation is mainly driven by a "chemical" mechanism, i.e. by a change of the ZnO stoichiometry during annealing. This kind of relaxation mechanism is now well recognized in oxide films [40]. In addition, it is well-known that ZnO films present oxygen vacancies VO [41-43] regardless of the deposition process. If VO is the dominant defect, it may induce large distortion in the ZnO wurtzite lattice. In fact, the large size of the oxygen ions helps to maintain the ZnO crystal structure so that oxygen vacancies induce large inward relaxation of the neighboring atoms and then high stresses [39]. As a consequence, we postulate that, similarly to what occurs in epitaxial ZnO films deposited by pulsed laser deposition [42], a variation of the oxygen vacancy concentration during heating (or ageing under air) involves a stress relaxation. This phenomenon is limited by the presence of

Si_3N_4 coatings preventing the diffusion of oxygen atoms through the ZnO films, and the Si_3N_4 diffusion barrier is operant up to 600°C.

The fact that the four cases are similar on Fig. 3 from the annealing at 800°C and during cooling suggests that a complete relaxation of as-deposited stresses (i .e. due to the growth process) may happen at 800°C. Thus the residual stress in ZnO at room temperature should be only thermal stresses due to the mismatch of the coefficients of thermal expansion of the film (α_f) and the substrate (α_S). If we assume a purely elastic behaviour during cooling and a perfect adhesion between thin film and substrate, the thermal stress σ_{Th} can be written as :

$$\sigma_{Th} = \frac{E_f}{1-\nu_f}(\alpha_f - \alpha_S)(T_i - T_f) \quad (3)$$

where E_f et ν_f are the Young's modulus and the Poisson's ratio of the film, T_i is the intial temperature (i.e. temperature of the plateau) and, T_f the final temperature (i.e. room temperature). If we consider a perfect (0001) fibre textured material, the cooling treatment should lead to a tensile stress state of about 680 MPa in the ZnO films. This calculated value is in good agreement with the ones obtained on both samples (about 600 MPa). The presented analysis leads to the same results for the two different samples after annealing at 800°C. We can conclude the Si_3N_4 layer is no more operant as a diffusion barrier at such temperature.

5. Conclusions

In summary, we have investigated residual stresses in sputter-deposited ZnO films on Si substrates with the use of XRD. Two kinds of films have been studied raw ZnO and ZnO encapsulated in Si_3N_4. First, we have shown that as-deposited ZnO films are both in a high compressive stress state (about -0.65 GPa). Stress relaxation upon annealing is observed: a

transition from compressive to tensile stresses has been evidenced at different temperatures during annealing up to 800°C. Thanks to in-situ XRD measurements, we have observed a significant microstructural evolution and stress relaxation in ZnO films during annealing. The comparison between annealing in Ar or air atmospheres allows us to highlight that the stress relaxation in ZnO films may be oxygen concentration dependent and, thus may be attributed to a variation of the oxygen vacancy concentration. This chemical stress relaxation mechanism is thermally activated and starts at 200°C to finish at 600°C. All the presented results show that the encapsulation limits the structural evolution and stress relaxation (which are then shifted toward higher temperature of about 200°C) and then constitutes an efficient protective barrier for the ZnO films up to 600°C.

Acknowledgments

The authors express their thanks to the French ANR program for financial support under project n° MATETPRO07_247145.

References

[1] S.J. Pearton, D.P. Norton, K. Ip, Y.W. Heo, T. Steiner, Prog. Mater. Sci. 50 (2005) 293.

[2] S.B. Zhang, S.-H. Wei, A. Zunger, Phys. Rev. B 63 (2000) 075205.

[3] C-S.Hsiao, S-Y. Chen, W-Li Kuo, C-C. Lin, S-Y. Cheng, Nanotechnology 19 (2008) 405608.

[4] S J. Kang, Y H. Joung, Appl. Surf. Sci. 253 (2007) 7330.

[5] B. Hwang, K. Park, H-S. Chun, C-H. An, H. Kim, H-J. Lee, Appl. Phys. Lett. 93 (2008) 222104.

[6] S.J. Chen, Y.C. Liu, C.L. Shao, C.S. Xu, Y.X. Liu, L. Wang, B.B. Liu, G.T. Zou, J. Appl. Phys. 99 (2006) 066102.

[7] P. Pant, J.D. Budai, J. Narayan Acta Materiala 58 (2010) 1097.

[8] J. Hinze, K. Ellmer, J. Appl. Phys. 88 (2000) 2443.

[9] C.S Chen, C.T Kuo, T.B. Wu, I.N. Lin, Jpn. J. Appl. Phys. 36 (1997) 1169.

[10] T. Hiramatsu, M. Furuta, H. Furuta, T. Matsuda, C. Li, T. Hirao, J. Cryst. Growth 311 (2009) 282.

[11] K. Haga, T. Suzuki, Y. Kashiwaba, H. Watanabe, B.P. Zhang, Y. Segawa, Thin Solid Films 433 (2003) 131.

[12] X.W. Sun, H.S. Kwok, J. Appl. Phys. 86 (1999) 408.

[13] A. Shikanai, T. Azuhata, T. Sota, S. Chichibu, A Kuramata and K. Horino et al., J Appl Phys 81 (1997) 417.

[14] R. Triboulet and J. Perrière, Prog. Cryst. Growth Charact. Mater. 47 (2003) 65.

[15] B.C. Mohanty, Y.H. Jo, D.H. Yeon, I.J. Choi, Y.S. Cho, Appl. Phys. Lett. 95 (2009) 062103.

[16] R. Ghosh, D. Basak, S. Fujihara J. Appl. Phys. 96 (2004) 2689.

[17] S. Kishimoto, T. Yamada, K. Ikeda, H. Makino, T. Yamamoto, Surf. Coat. Technol. 201 (2006) 4000.

[18] Lin, S.S., Huang, J.-L., Lii, D.-F, Surf. Coat. Technol. 176 (2004) 173.

[19] Yu, H.-W., Du, Y.-L., Wang, J., Yan, X.-A., Gao, B., Fangzhi Gaoxiao Jichukexue Xuebao, 22(1) (2009) 102.

[20] M.K. Puchert, P.Y. Timbrell, R.N. Lamb, J. Vac. Sci. Technol. A 14 (1996) 2220.

[21] I. Ozen, M.A. Gulgun, Adv. in Sci. and Technol. 45 (2006) 1316.

[22] Y.S. Touloukian, R.K. Kirby, R.E. Taylor, T.Y.R. Lee "Thermophysical properties of matter", vol 13. Thermal expansion nonmetallic solids.New York: IFI/Plenum, p. 176

[23] R-S. Chu, S-T. Shiue, Thin Solid Films 517 (2009) 4879.

[24] F. Vacandio, Y. Massiani, P. Gergaud, O. Thomas, Thin Solid Films 319 (2000) 9.

[25] R. Polini, G. Mattei, R. Walle, F. Casadei, Thin Solid Films 515 (2006) 1011.

[26] V. Hauk, "Structural and residual stress analysis by nondestructive methods", Elsevier, 1997

[27] J. Tranchant, P.Y. Tessier, J.P. Landesman, M.A. Djouadi, B. Angleraud, P.O. Renault, B. Giraud, P. Goudeau, Surf. Coat. Technol. 202 (2008) 2247.

[28] G.G. Stoney, Proc. Soc. Lond. A82 (1909) 172.

[29] P. Van Houtte, L. De Buyser, Acta Metall. Mater. 41(2) (1993) 323.

[30] C.V. Thompson, Annual Rev. Mater. Sci. 30 (2000) 159.

[31] I. Petrov , P.B. Barna, L. Hultman, J.E. Greene, J. Vac. Sci. Technol. A 21 (2003) 117.

[32] D. Faurie, P.-O. Renault, E. Le Bourhis,P. Goudeau, Acta Materialia 54 (2006) 4503.

[33] H. Ledbetter and A. Migliori, J. Appl. Phys. 100 (2006) 063516.

[34] D. Faurie, P.-O. Renault, E. Le Bourhis,P. Goudeau, J. Appl. Phys. 98 (2005) 093511.

[35] J.I. Langford, J. Appl. Crystallogr. 11 (1978) 10.

[36] O. Kappertz, R. Drese, M. Wuttig, J. Vac. Sci. Technol. A 20 (2002) 2084.

[37] R. Drese, M. Wuttig, J. Appl. Phys. 98 (2005) 073514.

[38] Y. Okada, Y. Tokumaru, J. Appl. Phys. 56 (1984) 314.

[39] A. Janotti, C.G. Van de Walle, Phys. Rev. B 76 (2007) 165202.

[40] F. Conchon, A. Boulle, R. Guinebretière, E. Dooryhée, J-L. Hodeau, C. Girardot, S. Pignard,

J. Kreisel, F. Weiss, L. Libralesso, T. L. Lee, J. Appl. Phys. 103 (2008) 123501.

[41] S. Dutta, S. Chattopadhyay, A. Sarkar, M. Chakrabarti, D. Sanyal, D. Jana, Prog. Mater. Sci. 54 (2009) 89.

[42] J. Zhao, L. Hu, W. Liu, Z. Wang, Appl. Surf. Sci. 253 (2007) 6255.

[43] K. Wang, Z. Ding, S. Yao, H. Zhang, S. Tan, F. Xiong, P. Zhang, Mater. Res. Bull. 43 (2008) 3327.

List of figure captions

Fig. 1: A few exemples of ex-situ θ/2θ diffractograms measured for x-ray stress analysis for the 100 nm thick encapsulated ZnO film before annealing. The legend reports the corresponding ψ angles (i.e. inclinaison of the sample).

Fig. 2: In situ θ/2θ diffractograms measured during annealing in air atmosphere for the 100 nm thick raw ZnO film.

Fig. 3. (0002) peak position as a function of temperature during heat treatment (from 30°C until 800°C) and after cooling (at 30°C) for ZnO/Si (full symbol) and for ZnO encapsulated by Si_3N_4 (open symbol). These XRD measurements were recorded in air (gray continuous lines) and argon (dotted black lines) atmospheres inside the furnace chamber.

Fig. 4: $\sin^2\psi$ plots of the (10-11) reflection for an encapsulated (a) and raw (b) ZnO film. The measurements are performed at room temperature after a given heat treatment (see legend). Open symbols represent experimental data with the associated error bars, straight-lines correspond to the linear fit.

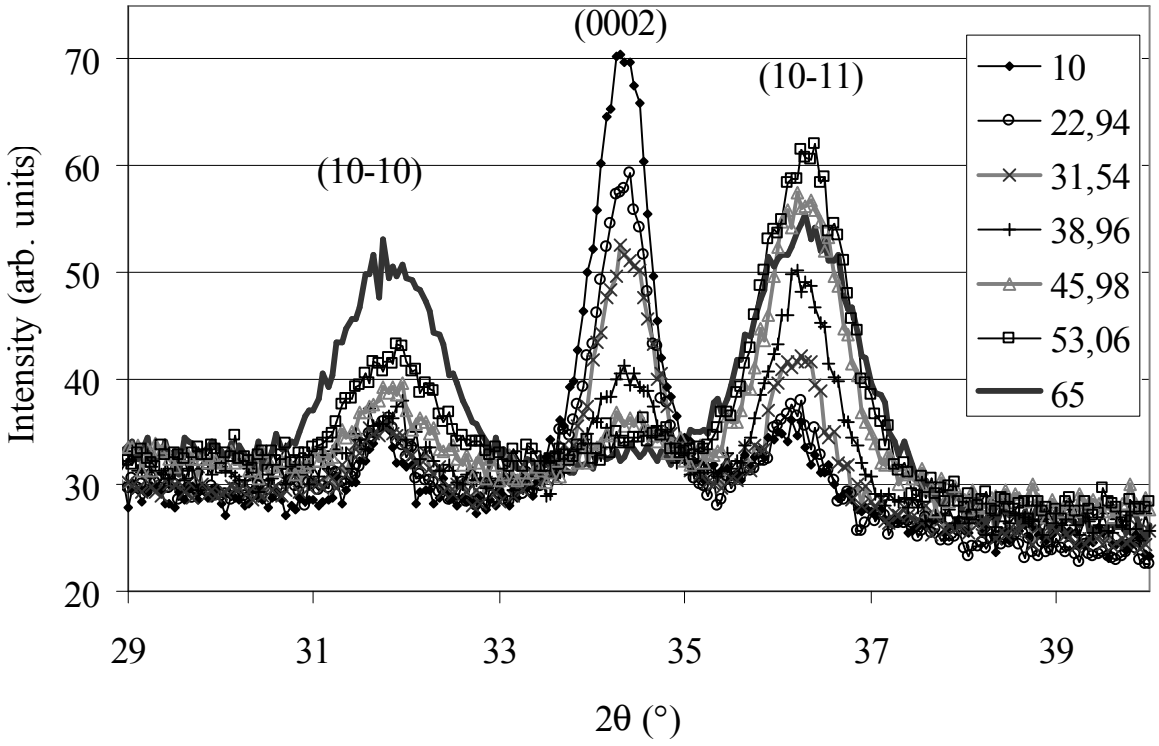
(0002)
(10-11)
(10-10)
Intensity (arb. units)
70
60
50
40
30
20
29
31
33
35
37
39
2θ (°)
10
22,94
31,54
38,96
45,98
53,06
65

Fig. 1

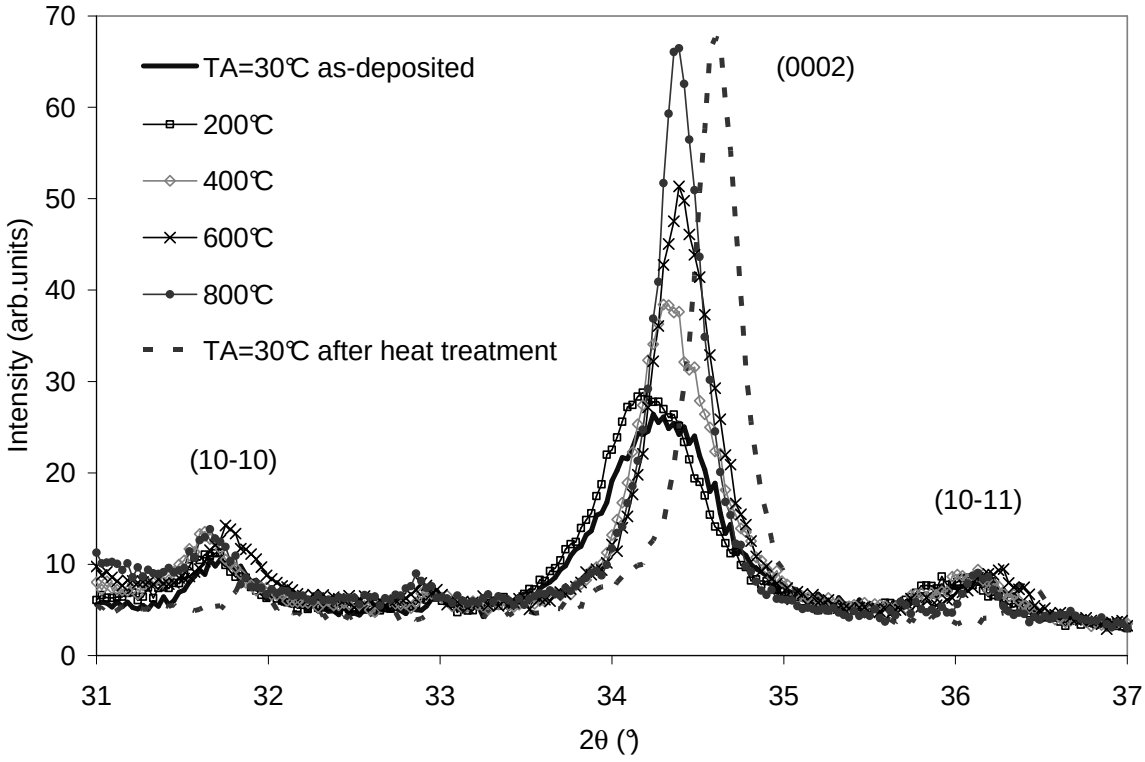
TA=30℃ as-deposited
200℃
400℃
600℃
800℃
TA=30℃ after heat treatment
(0002)
(10-10)
(10-11)
Intensity (arb.units)
2θ (°)
0
10
20
30
40
50
60
70
31
32
33
34
35
36
37

Fig. 2

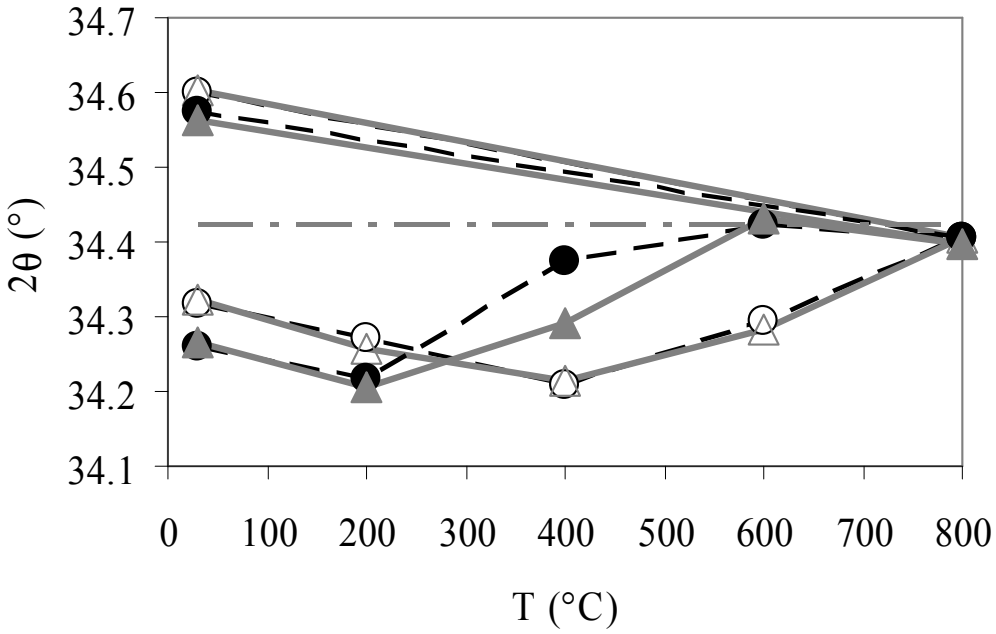
34.7
34.6
34.5
34.4
34.3
34.2
34.1
2θ (°)
0
100
200
300
400
500
600
700
800
T (°C)

Fig. 3

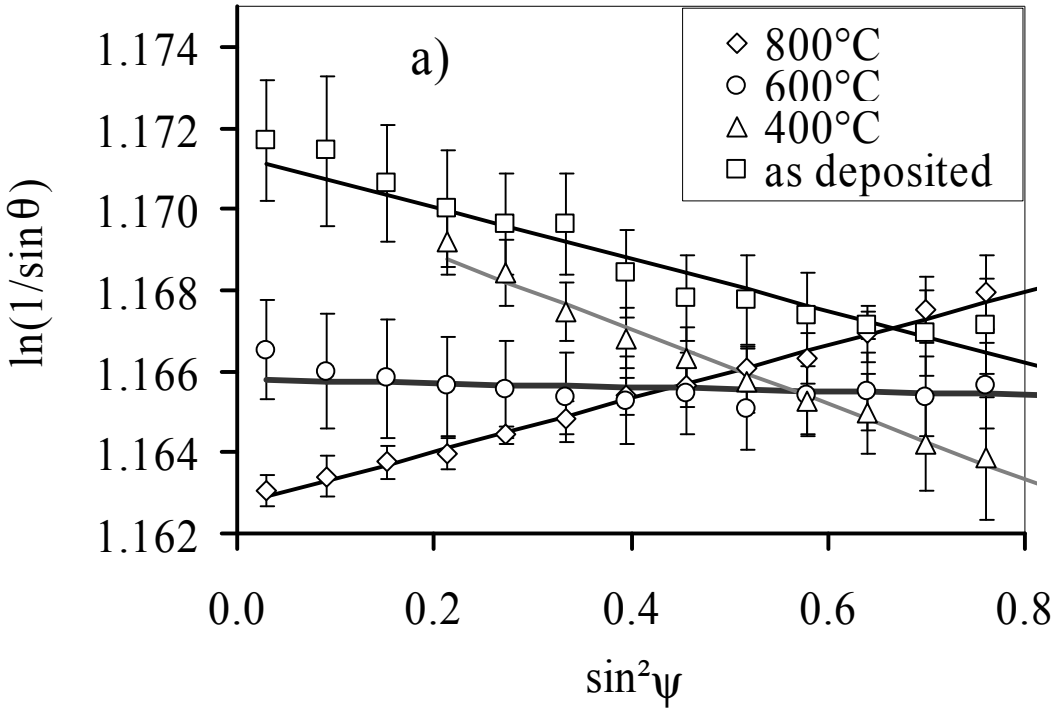
a)
800°C
600°C
400°C
as deposited
1.174
1.172
1.170
1.168
1.166
1.164
1.162
ln(1/sinθ)
0.0
0.2
0.4
0.6
0.8
sin²ψ

Fig. 4.a

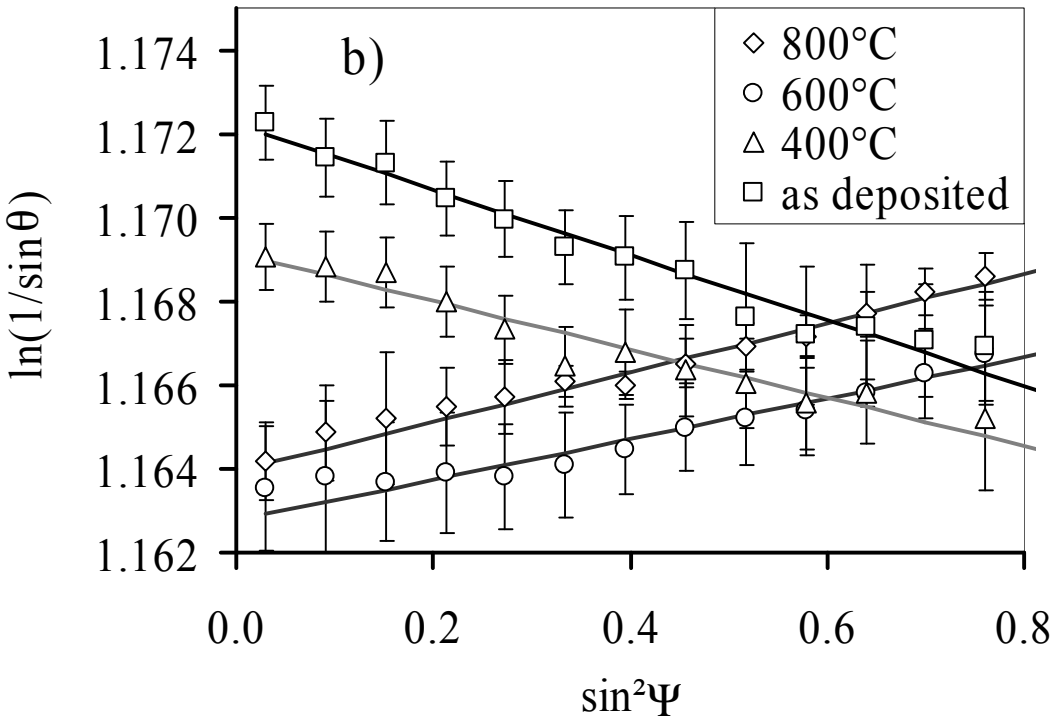
b)
800°C
600°C
400°C
as deposited
1.174
1.172
1.170
1.168
1.166
1.164
1.162
ln(1/sinθ)
0.0
0.2
0.4
0.6
0.8
sin²Ψ

Fig. 4.b